Supporting Information

Reconstruction of Bimetal $CoFe_{0.13}$-MOF to Enhance the Catalytic Performance in Oxygen Evolution Reaction

Kexin Yang[1] ‡, Zeqi Jin[1]‡, Qicheng Zhang[1], Qiming Chen[1], Wenchao Peng[1,2], Yang Li[1,2], Fengbao Zhang[1], Qing Xia[1], Xiaobin Fan[1,2]**

[1]School of Chemical Engineering and Technology, State Key Laboratory of Chemical Engineering, Collaborative Innovation Center of Chemical Science and Engineering, Tianjin University, Tianjin, 300072, China.
[2]Chemistry and Chemical Engineering Guangdong Laboratory, Shantou, 515031 China.
School of Chemical Engineering and Technology, State Key Laboratory of Chemical

Corresponding Author

*Xiaobin Fan

Email: xiaobinfan@tju.edu.cn

*Qing Xia

Email: xiaqing@tju.edu.cn

Contents:

Experimental Details

Synthesis of the $CoFe_{0.13}$-MOF:

2-6 naphthalene dicarboxylic acid (165 mg) and Ferrocenecarboxylic acid (23 mg) were dissolved in 5 mL DMF and 1 mL NaOH (0.4 M) was added. Then the solution was mixed slowly with 5 mL DMF solution containing cobalt (II) nitrate nonahydrate (218 mg) in a 30 mL Teflon-lined stainless-steel autoclave. The Teflon-lined stainless-steel autoclave was heated for 15 h at 100 °C. The resulting products were washed with DMF and ethanol for three times and dried naturally.

OER reconstruction:

The Amperometric i-t Curve program was run for 50000s in 1M KOH alkaline solution with an initial current of 10 mA cm^{-2}, followed by rinsing with deionized water, and drying naturally to obtain deactivated $CoFe_{0.13}$-MOF, namely, $CoFe_{0.13}O_xH_y$.

Solvothermal reconstruction:

The process of synthesizing $CoFe_{0.13}$-MOF was repeated without adding 2-6 naphthalene dicarboxylic acid, Ferrocenecarboxylic acid and cobalt (II) nitrate nonahydrate. Finally, the refreshed $CoFe_{0.13}O_xH_y$, is named as re-$CoFe_{0.13}O_xH_y$.

Materials characterization. The phases in each sample were detected by X-ray diffraction (XRD, Bruker D8 Advanced, Germany). The molar ratio of Co:Fe was measured by inductively coupled plasma mass spectrometry (ICP-OES:Shimadzu ICPE-9800).The morphology and microstructure were examined by transmission electron microscopy (TEM, JEM-2100), scanning electron microscopy (SEM, S4800) equipped with an energy-dispersive X-ray analyzer (EDS). The chemical states of samples were concluded by X-ray photoelectron spectroscopy (XPS, ESCALAB 250 XI). electron spin resonance (ESR) spectra were conducted on Bruker EMX PLUS.

Electrochemical measurements. All the electrochemical data were collected from a CHI760E electrochemical workstation. A standard three–electrode cell was used with 1 M KOH as the electrolyte. Ag/AgCl (3.5 M KCl solution) electrode and a graphite rod were chosen as reference and counter electrodes, respectively. All the linear sweep voltammetry (LSV) data were recorded at a scan rate of 5 mV s^{-1}. Time–dependent current density curves were obtained by chronoamperometric measurements. The electrochemical impedance spectroscopy (EIS) results were determined at 0.5 V vs. Ag/AgCl, and the corresponding frequency range is 0.1~10^6 Hz.

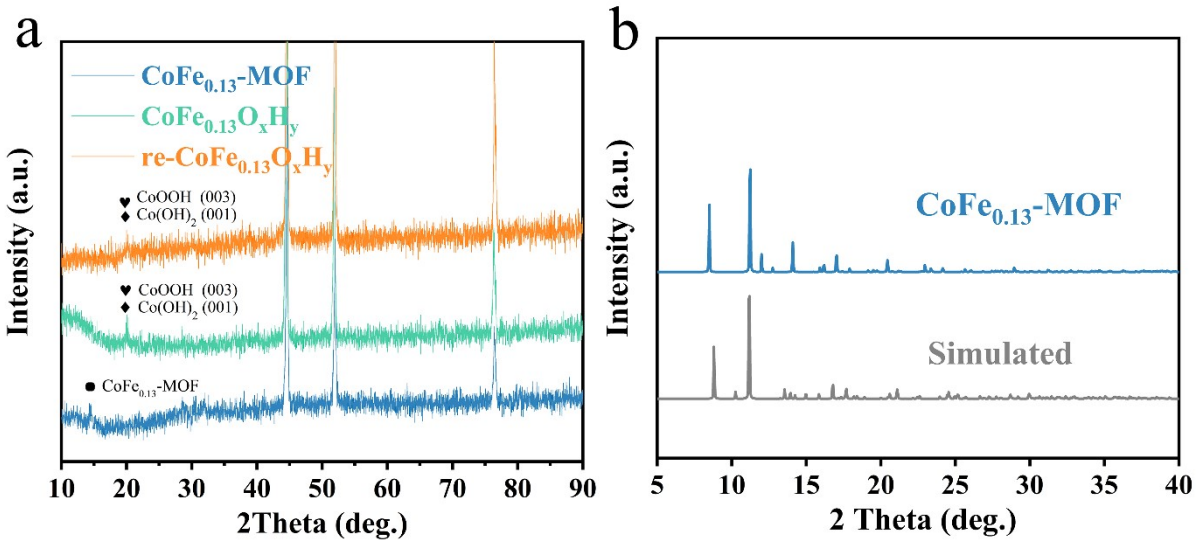

Fig. S1 (a) XRD patterns of the prepared $CoFe_{0.13}O_xH_y$, re-$CoFe_{0.13}O_xH_y$ and $CoFe_{0.13}$-MOF. The crystal structure of CoOOH and $Co(OH)_2$ is shown in the inset. (b) XRD patterns of the $CoFe_{0.13}$-MOF control sample without the presence of nickel foam and the simulated XRD pattern from previous study.

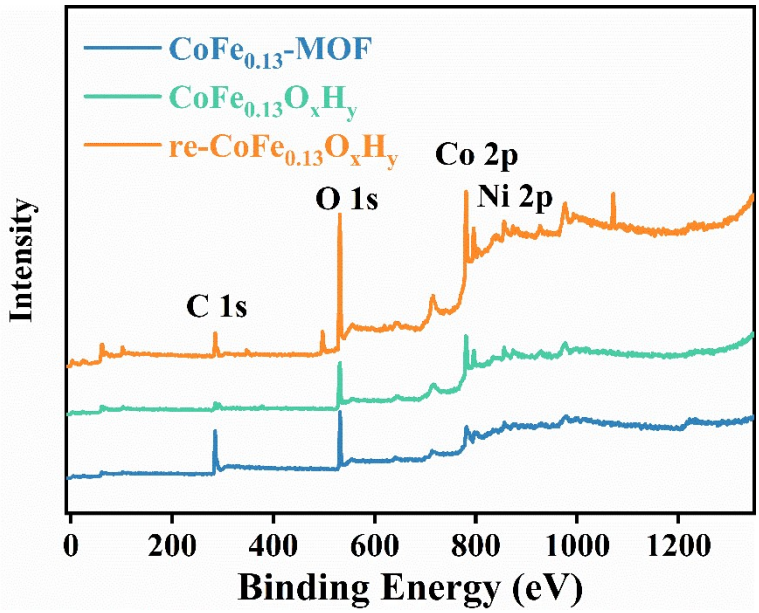

Fig. S2 The full range XPS spectra, the peaks of C 1s, O 1s, Co 2p and Ni 2p are detected.

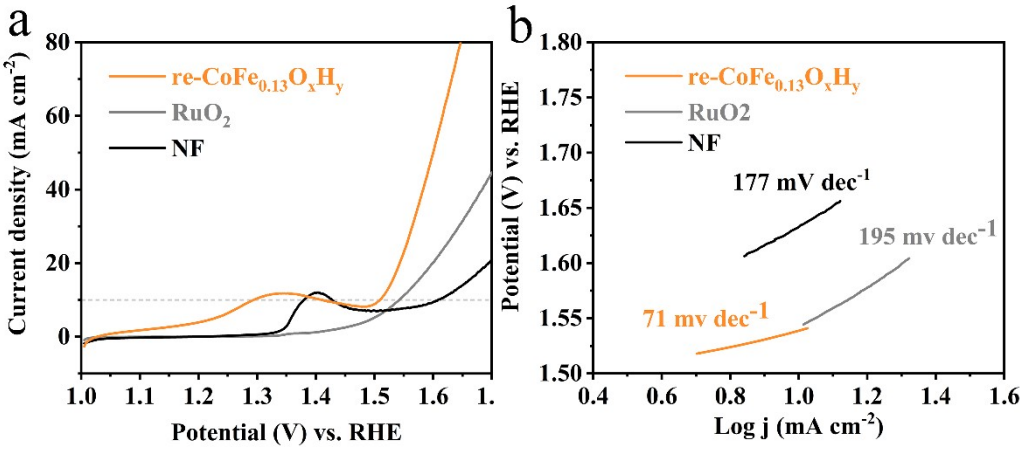

Fig. S3. Electrochemical characterization of re-$CoFe_{0.13}$-MOF, commercial RuO_2 and the Ni foam. **(a)** Polarization curves. **(b)** Tafel slopes.

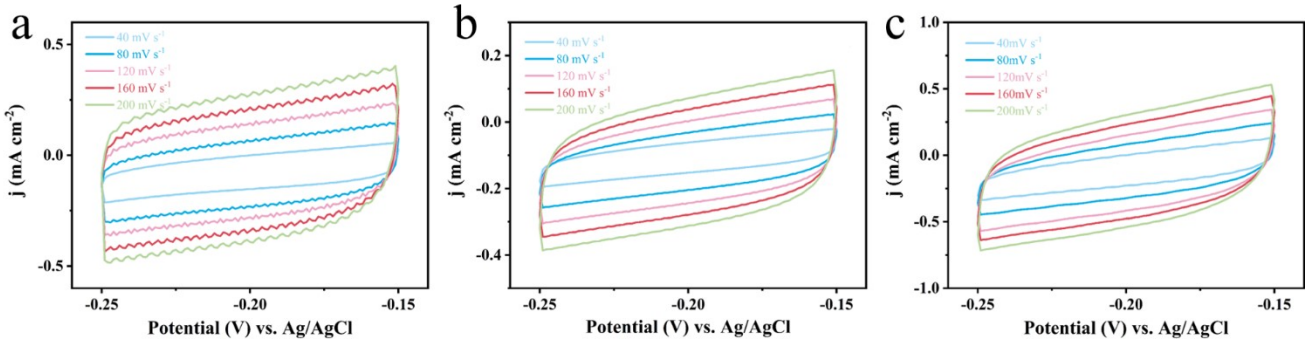

Fig. S4. Corresponding CV curves in non-Faraday region. CV cycling of **(a)** $CoFe_{0.13}$-MOF, **(b)** $CoFe_{0.13}O_xH_y$ and **(c)** re-$CoFe_{0.13}O_xH_y$ in 1 M KOH from 40 mVs^{-1} to 200 mVs^{-1}.

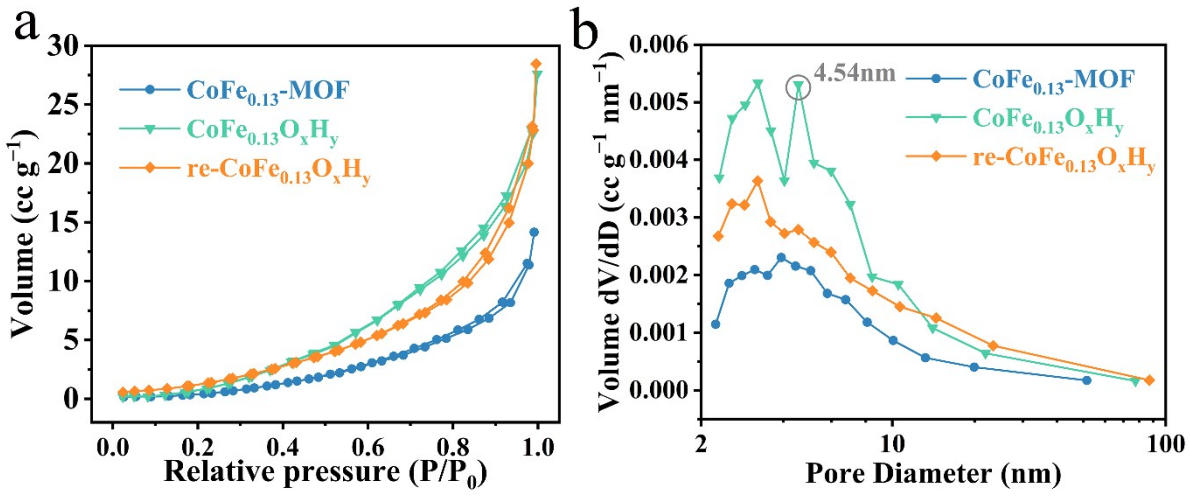

Fig. S5 The pore structure characterization of the $CoFe_{0.13}$-MOF, $CoFe_{0.13}O_xH_y$, and re-$CoFe_{0.13}O_xH_y$ **(a)** N_2 sorption isotherms, and **(b)** pore size distribution curves.

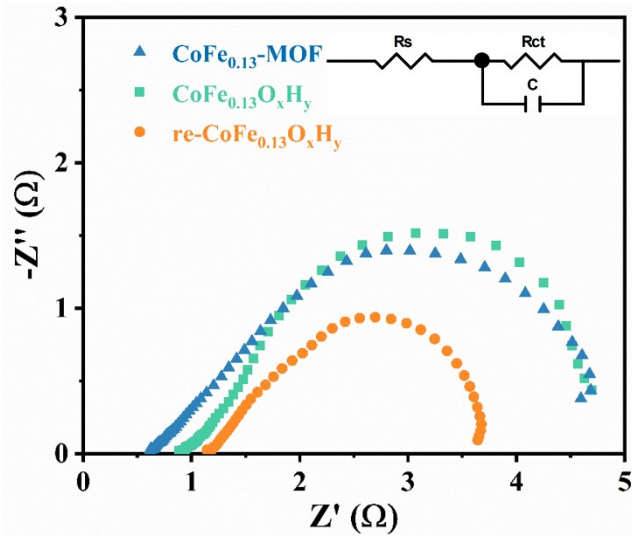

Fig. **S6** Nyquist plots. The re-$CoFe_{0.13}O_xH_y$ suggests a smaller charge transfer resistance (~2.5 Ω) than that of $CoFe_{0.13}$-MOF (~4 Ω) and $CoFe_{0.13}O_xH_y$ (~4 Ω).

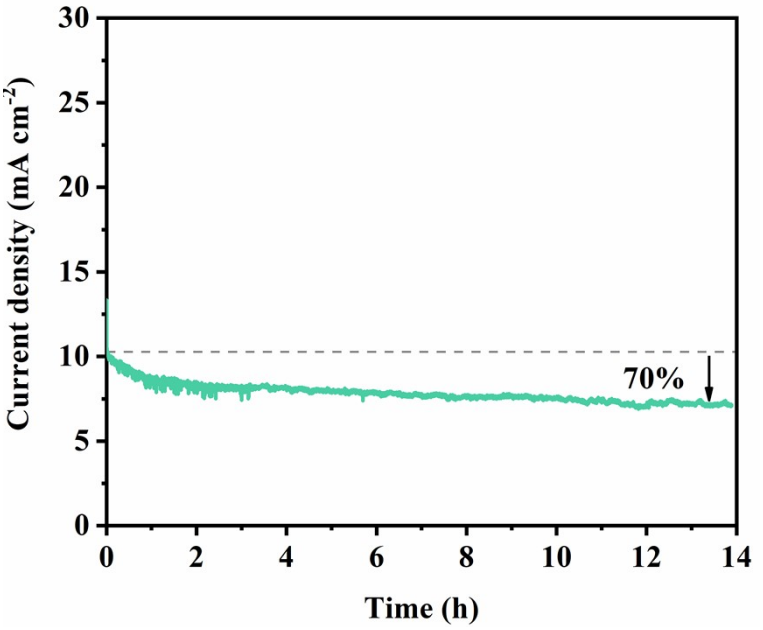

Fig. S7 Stability test of the original $CoFe_{0.13}$-MOF. The current density of the $CoFe_{0.13}$-MOF drops to 70% in 50000s.

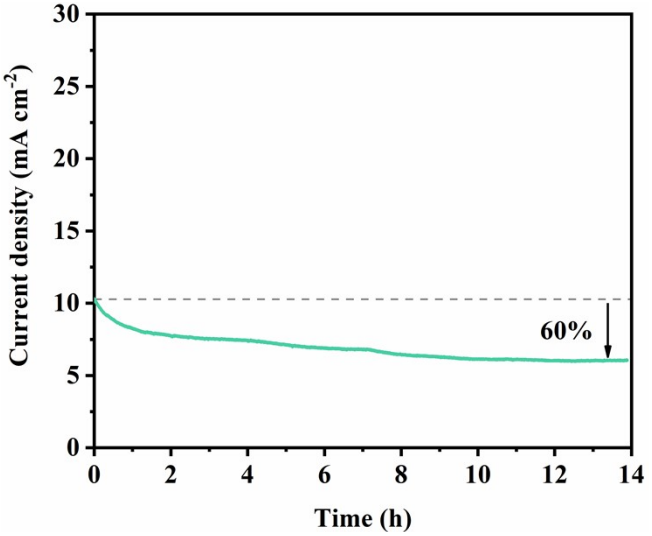

Fig. S8 Stability test of the $CoFe_{0.13}$-MOF-30h. The current density of the $CoFe_{0.13}$-MOF-30h drops to 60% in 50000s.

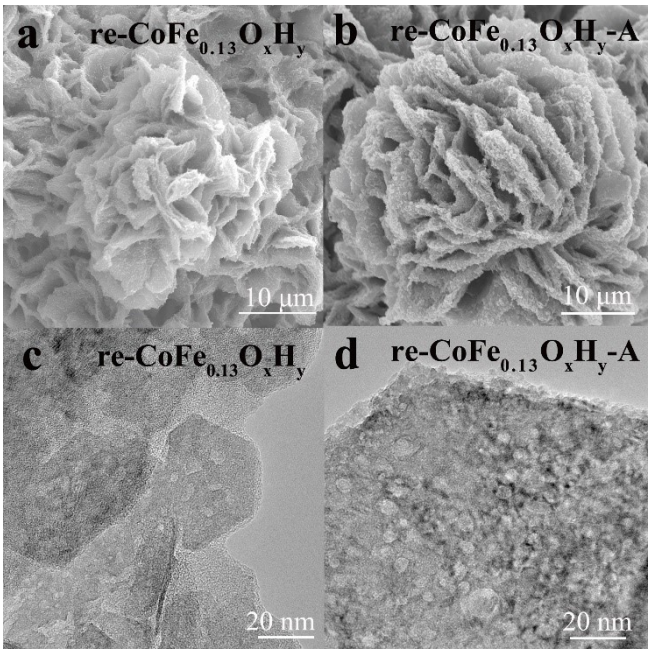

Fig. S9 Morphology of re-$CoFe_{0.13}O_xH_y$ after stability test. SEM images of (a) re-$CoFe_{0.13}O_xH_y$ and (b) re-$CoFe_{0.13}O_xH_y$-A. TEM images of (c) re-$CoFe_{0.13}O_xH_y$ and (d) re-$CoFe_{0.13}O_xH_y$-A.

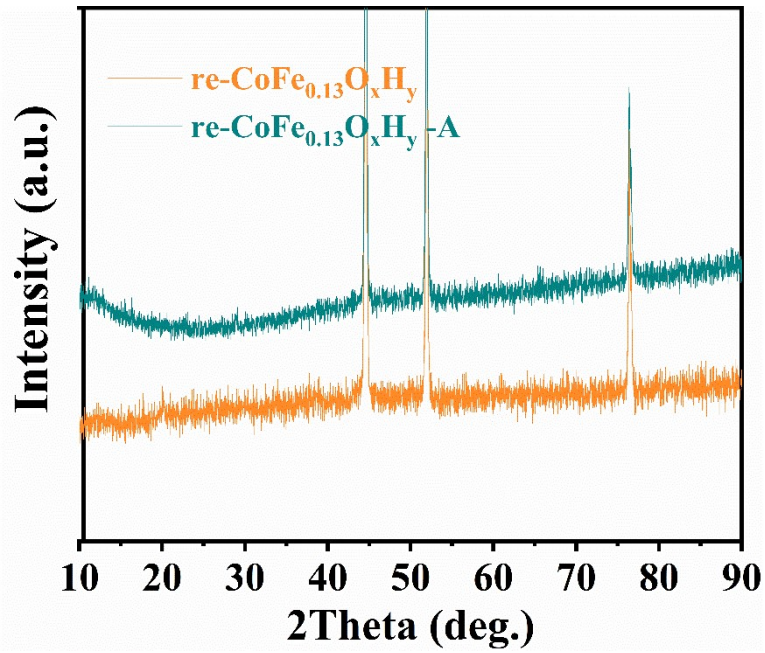

Fig. S10 XRD patterns of the prepared re-$CoFe_{0.13}O_xH_y$-A (the re-$CoFe_{0.13}O_xH_y$ after 85 h OER process).

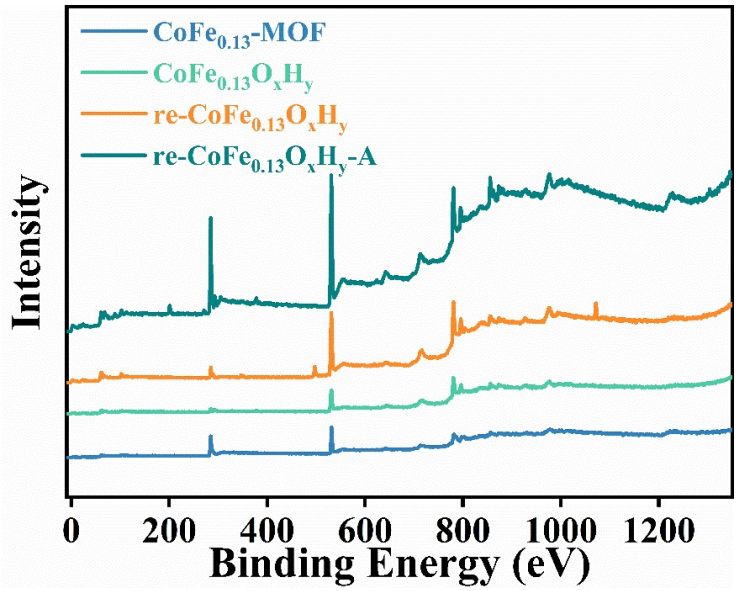

Fig. S11 The full range XPS spectra of the re-$CoFe_{0.13}O_xH_y$-A (the re-$CoFe_{0.13}O_xH_y$ after 85 h OER process).

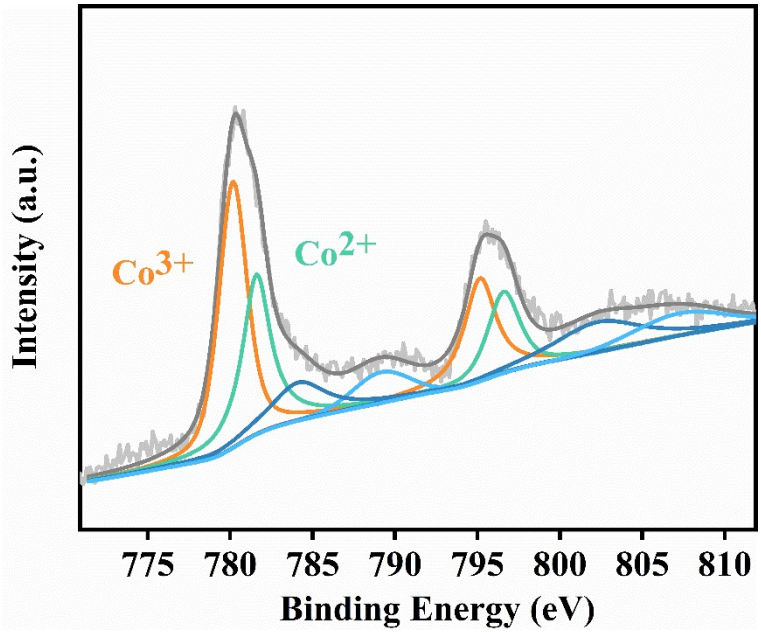

Fig. S12 The Co 2p XPS spectra of the re-$CoFe_{0.13}O_xH_y$-A (the re-$CoFe_{0.13}O_xH_y$ after 85 h OER process). The ratio of Co^{2+} to Co^{3+} is 0.77.

Tab. S1 The element content in the $CoFe_{0.13}$-MOF.

Element	Content[a] wt (%)
Co	4.49
Fe	0.388

[a]The data were measured by inductively coupled plasma mass spectrometry (ICP-EOS).

Tab. S2 XPS surface element content of the $CoFe_{0.13}$-MOF

Name	Atomic %
C1s	60.54
O1s	29.52
Fe2p3	0.62
Ni2p3	2.22
Co2p3	7.09

Tab. S3 Comparison of stability with other MOF catalysts.

Catalyst	Test Condition	Stability Performance
This work	1 M KOH, 10 mA cm^{-2}	85.0 h
CoFe-BDC[1]	1 M KOH, 10 mA cm^{-2}	< 1.0 h
ZIF-67(002) [2]	1 M KOH, 10 mA cm^{-2}	8.0h
$Co_{0.6}Fe_{0.4}$-MOF-74[3]	1 M KOH, 10 mA cm^{-2}	12.0h
CoBDC-Fc[4]	1 M KOH, 100 mA cm^{-2}	80.0h
CoOOH[5]	1 M KOH, 10 mA cm^{-2}	100h
γ-CoOOH[6]	1 M KOH, 10 mA cm^{-2}	13.0h
F-CoOOH/NF[7]	1 M KOH, 30 mA cm^{-2}	10.0h
FeCoOOH[8]	1 M KOH, 10 mA cm^{-2}	15.0h

Reference

1. J. Xu, X. Zhu and X. L. Jia, *Acs Sustainable Chemistry & Engineering*, 2019, **7**, 16629-16639.
2. J. W. Wan, D. Liu, H. Xiao, H. P. Rong, S. Guan, F. Xie, D. S. Wang and Y. D. Li, *Chemical Communications*, 2020, **56**, 4316-4319.
3. X. H. Zhao, B. Pattengale, D. H. Fan, Z. H. Zou, Y. Q. Zhao, J. Du, J. E. Huang and C. L. Xu, *Acs Energy Letters*, 2018, **3**, 2520-2526.
4. Z. Hu, S. L. Shi, L. Wang, S. J. Chen, Y. S. You, S. H. Wang and C. Chen, *Applied Surface Science*, 2020, **528**.
5. J. Zhou, Y. Wang, X. Z. Su, S. Q. Gu, R. D. Liu, Y. B. Huang, S. Yan, J. Li and S. Zhang, *Energy & Environmental Science*, 2019, **12**, 739-746.
6. J. H. Huang, J. T. Chen, T. Yao, J. F. He, S. Jiang, Z. H. Sun, Q. H. Liu, W. R. Cheng, F. C. Hu, Y. Jiang, Z. Y. Pan and S. Q. Wei, *Angewandte Chemie-International Edition*, 2015, **54**, 8722-8727.
7. P. Z. Chen, T. P. Zhou, S. B. Wang, N. Zhang, Y. Tong, H. X. Ju, W. S. Chu, C. Z. Wu and Y. Xie, *Angewandte Chemie-International Edition*, 2018, **57**, 15471-15475.
8. T. T. H. Nguyen, J. Lee, J. Bae and B. Lim, *Chemistry-a European Journal*, 2018, **24**, 4724-4728.